Flow-Induced Bending Deformation of Electrospun Polymeric Filtration Membranes Using the "Leaky" Bulge Test

Temitope Q. Aminu, David F. Bahr

School of Materials Engineering, Purdue University, West Lafayette, IN 47907, U.S.A.

ABSTRACT

In service, hydraulic flow is usually perpendicular to the plane of electrospun fiber mats for water filtration, inducing an out-of-plane deformation. In this paper, we have investigated the out-of-plane deformation response of wet electrospun polyacrylonitrile fiber mats with distinct average constituent fiber diameters of 232 ± 36 nm, 727 ± 148 nm and 1017 ± 80 nm, but with nominally similar thicknesses and areal densities using the classical bulge testing technique. The resultant pressure-deflection relationships are incompatible with constitutive models for out-of-plane deformation of continuum materials. Rather, the fiber mats exhibited a one-half dependence ($p \sim h^{\frac{1}{2}}$) governed by fiber deflection, and pressure asymptote indicative of steady-state fluid percolation, but influenced by the mats areal densities. In addition, the apparent bending rigidity increased with increasing fiber diameter. In the range tested for fiber mats with average fiber size of 232 nm, increases in mat thickness did not noticeably alter the measured rigidities, although a slight increase in pressure asymptote is observed. Cyclic flow rate tests provided evidence of good recoverability as well as minimal topological modifications.

Author accepted copy: Polymer, vol. 235, paper 124274 (8 pages) (2021) DOI: 10.1016/j.polymer.2021.124274

1. Introduction

Non-woven polymer network structures generated from the electrospinning process, consisting of fibrous structures tracing microscopically intricate and tortuous paths, present unique systems wherein derived functionalities are predicated on the consolidation of material properties and performance at all levels of structural hierarchy, giving rise to novel, and in some instances, nontraditional material solutions that have been deployed in a variety of applications [1]. For instance, single fibers possess high aspect ratios that, in turn, confer high surface area-to-volume ratios, providing robust miniature substrates that act as support for functional nanomaterials for sensing, detection and modulation of physical or chemical phenomena [1, 2]. Macroscopically, the random, layered and serpentine configuration of manifold electrospun fibers create considerably integrated web-like or network architectures that approximate open cell foams with high porosity. Coupling of the high surface area and flexibility of constituent fibers with the porous nature of the resulting non-woven structures has enabled the utility of these materials to span staggeringly diverse fields: from biomimetic applications in scaffold design for tissue engineering [3], to acting as barriers for size exclusion in filtration membranes [4].

By definition, non-woven fibrous architectures are not monolithic materials in the classic sense, and as such, they are subject to peculiar deformation mechanisms that distinguishes their response to mechanical stressors, even when measures for structural consolidation are imparted (via chemical, thermal or mechanical methods [5]). Expectedly, given the high density of network entanglements, fiber flexibility, and the relatively unconstrained degrees of freedom afforded to individual fibers with respect to mobility, the mechanical properties of non-woven fibrous structures are dominated by a complex mix of topological, tribological, and material factors. In terms of topology, fiber curvature, degree of alignment, fiber dimension, porosity, aspect ratio as well as number of fiber-fiber contact points are important determinants of overall mechanical properties of electrospun mats [6, 7]. Furthermore, through constitutive continuum models, tribology effects like fiber slippage and inter-fiber friction have been identified as playing a role in irrecoverable network texture evolution during deformation[8]. Elastic moduli of individual fibers, inter-fiber bonding and underlying polymer chemistry represent contributing material factors [6, 9, 10].

In water filtration applications, electrospun fiber mats are typically utilized as part of a layered composite structure of nonwovens [11] or as standalone unbonded/junction-bonded structures [12, 13]. In most filtration characterization procedures as well as in actual service, the mats are placed on multiply perforated supports, and hydraulic flow is channeled orthogonally to the

Author accepted copy: Polymer, vol. 235, paper 124274 (8 pages) (2021) DOI: 10.1016/j.polymer.2021.124274

plane of the mat, causing transverse compression. The compressibility of electrospun fiber mats induced by water flow is well documented [12, 14]. Another structural modification occurring in parallel, with or without a porous support, is the out-of-plane flow-induced deformation or bending that reconfigures the fibrous architecture, altering their size exclusion properties. For example, deformation induced by transmembrane pressure has been proposed to increase the pore sizes of electrospun filters for microfiltration applications, reducing its removal efficiency for bacterial cells [15]. Hence, alongside appraisal of filtration performance, understanding mechanical properties in the context of structural rigidity for effective resistance against hydraulic flow-induced deformation, against a backdrop of the aforementioned multiplicity of influencing factors, will help in establishing more robust structure-performance relationships for nonwoven fibers mats, and identifying parameters that ensure that material designs are adapted for water filtration as well as functional filtration membranes e.g. fluorescent chemosensory membranes [16].

An immediate presumption that figures prominently in the characterization of nonwoven mats is the dependence of macroscopic mechanical behavior on the constitutive fibers. For example, a predictive analytical model that expresses tensile strength of an electrospun nanofiber mat as a function of the tensile strength of single fiber has been established [17]. Experimentally, for single electrospun fibers, techniques based on atom force microscopy (AFM) and microelectromechanical systems (MEMS) have been utilized for the extraction of mechanical information [18-20]; and conventional macro-tensile tests are typically used in evaluating the macroscopic tensile behavior of nonwoven mats. Specifically, uniaxial tensile deformation tests reveal elastic-plastic stress-strain behaviors for electrospun fiber mats in general, irrespective of underlying fiber chemistry or initial fiber configuration [21-23] (the elastic-plastic nomenclature commonly used as descriptor for the deformation response of electrospun mats is derived from the likeness of the graphical curve to that observed for continuum materials; however, in a stricter sense, irreversible topological changes manifest instantaneously with deformation [7], and this should preclude the macroscopic “elasticity” characterization). In the same vein, mechanical assessment based on planar biaxial tensile tests have been carried out on electrospun sheets [24, 25]. Unlike uniaxial tests where fibers inevitably reorient in the loading direction, the random configuration of the fibers are largely preserved in this testing configuration [26, 27].

One mechanical characterization method based on out-of-plane deformation that, in principle, will preserve the random fiber assembly of electrospun mats, and at the same time, mimic flow-induced deformation is the hydraulic bulge test [28]. Conventionally designed for the

Author accepted copy: Polymer, vol. 235, paper 124274 (8 pages) (2021) DOI: 10.1016/j.polymer.2021.124274

characterization of elastic continuums, the bulge test is based on application of uniform lateral pressure to a free-standing film clamped over an orifice; and in response, the film undergoes a commensurate out-of-plane deflection or "bulge". The resulting pressure-deflection behavior is representative of the mechanical properties of the film. Classically, this technique has been adapted for the determination of biaxial modulus and residual stress in the thin films of metallic, semi-conductor and dielectric materials [29], under the assumptions of perfectly cylindrical or spherical bulge profiles (depending on sample geometry)[30]. However, the versatility of the bulge testing instrumentation has expanded its utility to testing of biological tissues [31], and materials for extreme environments [32]. More pertinently, the underlying deformation mechanics are consistent with classical membrane and plate models for continuum materials that can be accordingly adapted for the extraction of mechanical properties like elastic moduli and bending rigidities.

In this current study, a "leaky" bulge testing instrumentation based on hydraulic pressurization system is implemented for the mechanical characterization of wet electrospun PAN fiber mats. The term "leaky" is consequent upon the fact that fiber mats, due to their porous nature, invariably permit the percolation of the testing liquid medium, while also undergoing proportionate deformation dictated by the peculiar material architecture. Electrospun polyacrylonitrile (PAN) fiber mats are considered in this work. Due to easy spinnability, chemical resistance, hydrophilicity, good mechanical performance and thermal stability, PAN is commonly used in the fabrication of electrospun filters/membranes for water filtration applications [33, 34]. The pressure-deflection plots for the electrospun fiber mats exhibit a sub-linear dependence in contrast to typical continuum material response: a cubic dependence indicative of membrane stresses, and a linear dependence indicative of pure bending. We discuss the limitations of the application of classical continuum models to the deformation mechanics of electrospun fiber mats. The effects of variations in fiber diameter, thickness and flow rate on the pressure-deflection relationships are investigated. While we have selected electrospinning in this study for the ability to easily control fiber diameter, the basic behavior should extend to other non-woven systems with similar fiber-fiber contacts.

2. Experimental Section

2.1. Electrospinning: Mat Production

PAN powders (Sigma-Aldrich, M_w=150000 g/mol, ρ = 1.18 g/cm^3) were dissolved in dimethylformamide, DMF, to make solutions with 9wt%, 11wt%, and 13wt% PAN concentration. Subsequently, 1 wt% Acetone was added to the resulting solutions. Acetone has

Author accepted copy: Polymer, vol. 235, paper 124274 (8 pages) (2021) DOI: 10.1016/j.polymer.2021.124274

been shown to mitigate or eliminate bead formation [35]**.** The solution was stirred continuously for 24 hrs at room temperature. The electrospinning solution was loaded into a 3 mL syringe with a 19 ga (ID = 0.8126 mm) needle. A 13 x 13 cm^2 Aluminum foil situated at a distance of 15 cm from the syringe tip, was the designated collector plate. A voltage generator (Model SL300, Spellman NY) supplied a constant DC voltage of 15 kV maintained between the collector plate and needle tip, creating an electric field strength of 100 kV/m. A Flow rate of 0.34 mL/hr was supplied by a syringe pump (Advance infusion pump series 1200). Table 1 summarizes the physical characteristics of the PAN fiber mats. Total collection time varied from 6 – 8 hours, to ensure uniformity in thickness across the different mat fiber diameters. 4 x 4 cm^2 coupons were cut from the aluminum foil, and fiber mats were subsequently peeled off. Mat thickness measurements were taken at 5 different spots with a B.C. Ames Dial gage with a 1 μm resolution. For microstructural characterization, the electrospun mats were coated with a thin layer of platinum in a Cressington (208HR) sputter coater at plasma current of 40 mA for 1 minute, and imaged in the FEI Nova Nano scanning electron microscope. Fiber orientation was determined using the Gaussian gradient structure tensor function in OrientationJ (ImageJ, National Institute of Health, MD, USA).

Table1: Properties of the electrospun PAN fiber mats

PAN Concentration (wt.%)	**Fiber Diameter (nm)**	**Average Mat Thickness (μm)**	**Sample No**	**Areal Density (g/m^2)**
9	232 ± 36	29-31	1	8.1
			2	10.7
			3	11.3
11	727 ± 148		1	6.5
			2	8.0
			3	10.6
13	1017 ± 80		1	9.3
			2	10.9

The areal densities are similar; and on a fiber diameter group level, they are statistically equal (based on single factor ANOVA, $F(2, 5) = 0.51$, $p = 0.63$). It is important to note that each sample was obtained from different electrospinning sessions. This will inevitably accommodate more topological variation. Mat porosities ranged from 75% to 81%, calculated through the gravimetric method.

2.2. **Bulge Testing Hardware Design and Operation**

A schematic of the bulge testing hardware is shown in figure 1. The devices are structured for the real-time acquisition of pressure and center-point displacement or deflection data of the fiber mats during testing. Broadly, the main components are syringe pump, pressure transducer,

Author accepted copy: Polymer, vol. 235, paper 124274 (8 pages) (2021) DOI: 10.1016/j.polymer.2021.124274

laser displacement sensor and data acquisition board. Hydraulic pressure is supplied and controlled by a programmable syringe pump (Advance infusion system series 1200) with a linear force of 22 lbs., and an adjustable flow rate ranging from 0.01 μl/min to 8.87 ml/min (accuracy of 3%). A 60 ml syringe containing deionized water as the testing liquid is installed in the syringe pump. Unless stated otherwise, the testing flow rate is 10 ml/hr. The pressurization protocol was optimized to mitigate the occurrence of trapped air bubbles in the conduit system and pressure chamber. To that end, the conduit hose material was made of translucent vinyl that aided the visual inspection of advancing water front as well as bubbles. For sample loading, the freestanding mats were anchored over an O-ring that encircles the orifice and subsequently clamped; placement is done when the chamber is fully filled with deionized water, and a slight surface tension-modulated bulge is observed in the advancing water front. To ensure mat tautness and an initial planar configuration, carbon adhesive tapes were used to secure and fix the edges of the mats prior to clamping. A valve is manually operated to zero out the slight pressure build-up that occurs during the clamping process. Pressure measurements were made with a pressure transducer (PX 309 – 50GV, Omega Engineering, Inc) with a range of 50 psi (344 kPa), a ratiometric output of 10 mV/V, ± 2% full scale accuracy. Signals from the transducer are proportionately amplified with a bridge input signal conditioner (DRG-SC-BG, Omega engineering, Inc.)

Author accepted copy: Polymer, vol. 235, paper 124274 (8 pages) (2021) DOI: 10.1016/j.polymer.2021.124274

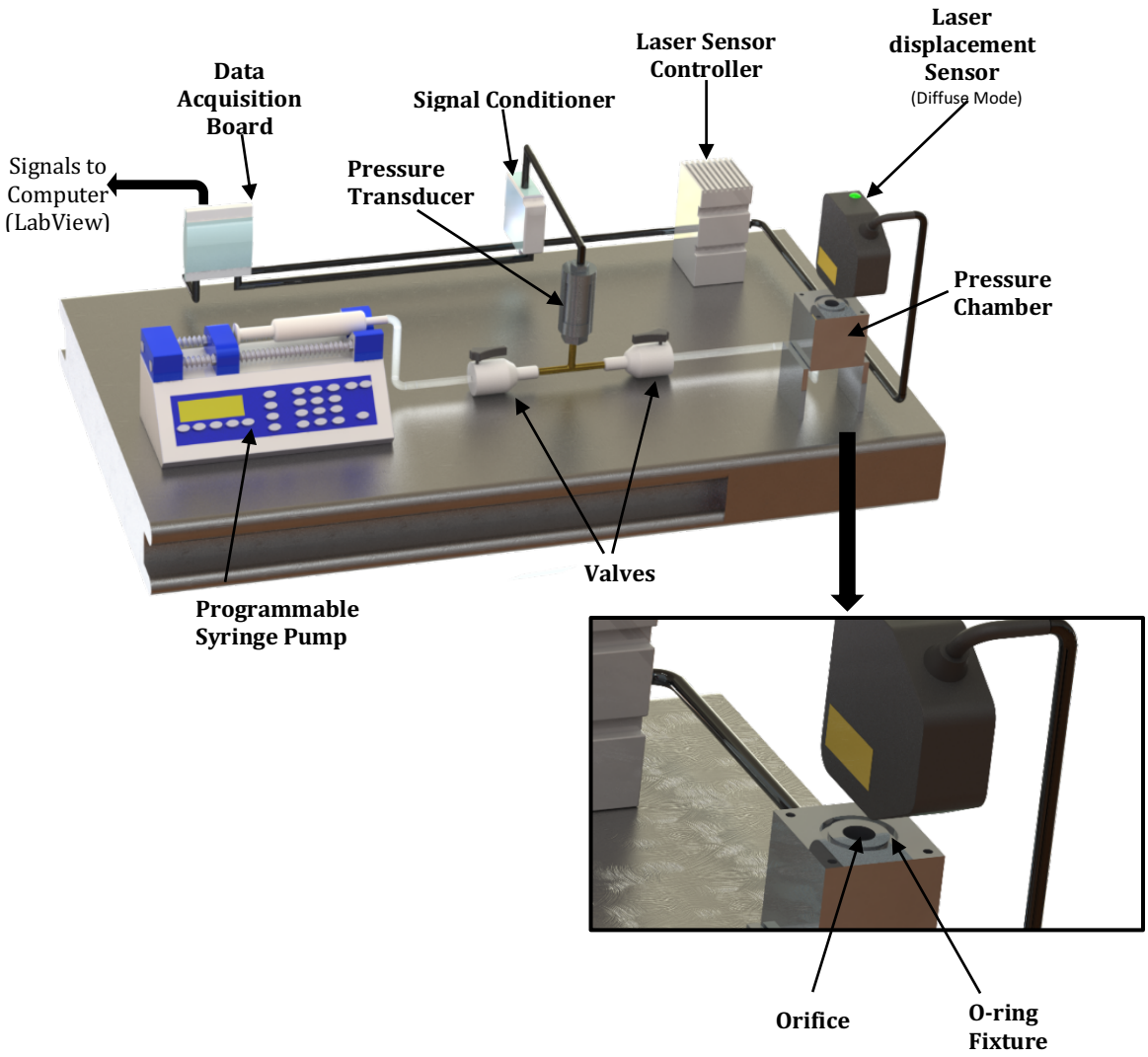

Figure 1: Schematic of "Leaky" bulge testing apparatus

Mat deflection is measured by 1D class II type triangulation laser (LK-G32, Keyence Corporation) with a wavelength of 655 nm, output of 0.95 mW and a spot size of 30 μm. The Laser spot was trained on the center of the mats at a working distance of 30 mm. Due to surface roughness of the fiber mats, the laser sensor was operated in diffuse mode for displacement data acquisition. Tests were terminated when the testing fluid had fully percolated through fiber mats and encroached on the laser spot. Synchronous collection of signals from the transducer and displacement sensor is made with an 8 channel data acquisition board (OM-USB-1608FS-PLUS, Omega engineering, Inc.). All analogue voltage signals were processed and pre-cleaned in the application development environment of LabView (National instruments).

Author accepted copy: Polymer, vol. 235, paper 124274 (8 pages) (2021) DOI: 10.1016/j.polymer.2021.124274

The system was verified for its ability to measure continuum membrane behavior by testing polyethylene and aluminum thin films, and was able to extract biaxial modulus, and by extension a young's modulus within 2 – 7% of the respective bulk materials.

3. Results and Discussion

Since electrospun mats are derived from continuous accumulation of unsystematically deposited single fibers strands, macroscopic mat behavior will be influenced by the resulting topology and properties of constituent fibers. Figure 2 shows rows containing the resultant microstructures, fiber diameter histograms and orientation distribution for the electrospun fiber mats produced from polymer solutions containing 9wt%, 11wt% and 13wt% PAN concentration.

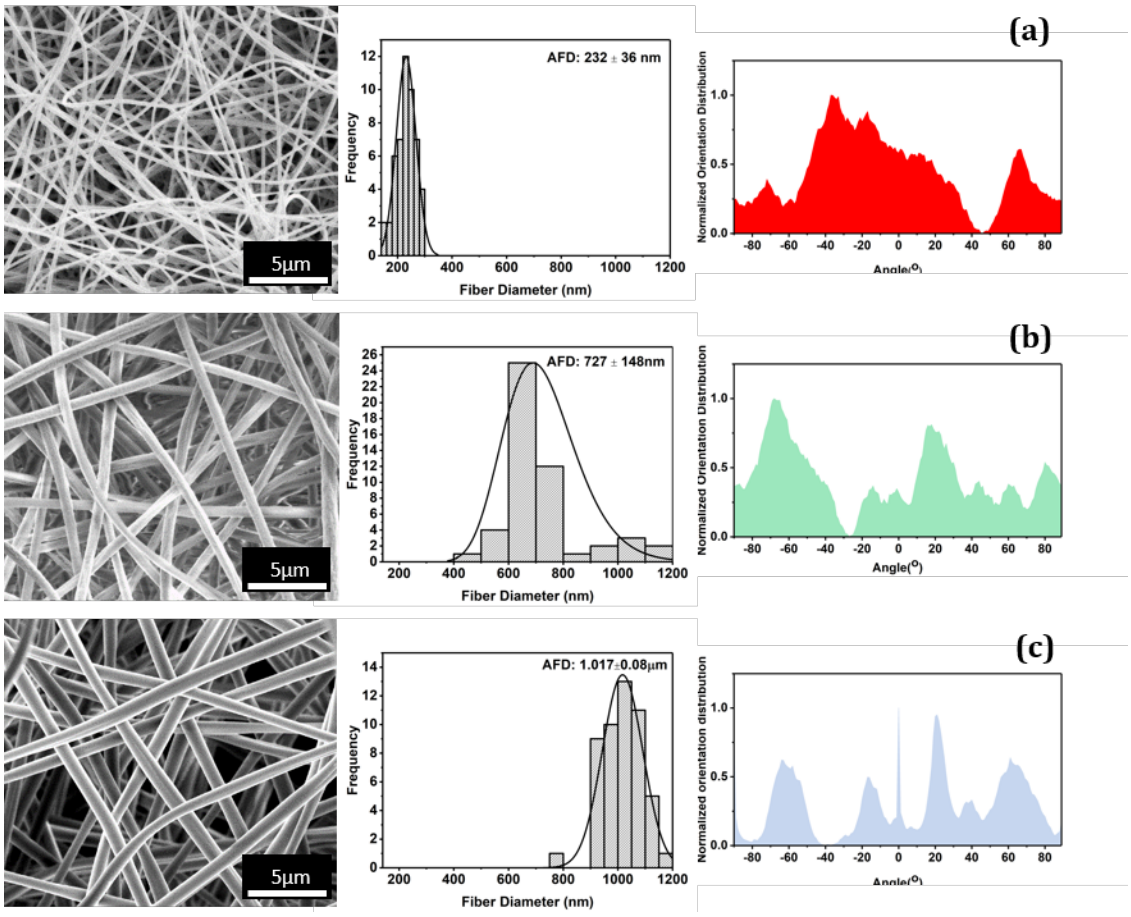

Figure 2: Micrograph, fiber diameter histogram and orientation distribution for electrospun solution formulations of (a) 9 wt% PAN (b) 11 wt% PAN (c) 13 wt% PAN (with 1wt% Acetone)

For these formulations, average fiber diameters were 232 ± 36 nm, 727 ± 148 nm and 1017 ± 80 nm respectively. Previous studies have established strong power law dependencies of the final diameters of electrospun PAN fibers on the polymer concentration, with scaling exponents ranging from 0.88 to 7.5 depending on PAN molecular weight [36, 37], indicating a strong

Author accepted copy: Polymer, vol. 235, paper 124274 (8 pages) (2021) DOI: 10.1016/j.polymer.2021.124274

correlation. In terms of topography, the fibers were relatively smooth with the unfavorable bead-on-string morphology effectively suppressed. Furthermore, from the micrographs, first image in each row of figure 2a, b and c, fiber tortuosity i.e. twists and turns, as well as overlap are observed to decrease with increasing fiber size. These may be ascribed to the countervailing effects of a progressively increasing fiber cross-section on in-flight bending and whipping instabilities during electrospinning. A lack of dominant directionality, as evidenced by the multiple peaks in the orientation distribution curves, third image in each row of figure 2a, b and c, underscores the random nature of fiber configuration.

3.1. General deformation response of fiber mats

Representative pressure-deflection plots for the electrospun fiber mats are shown in figure 3.

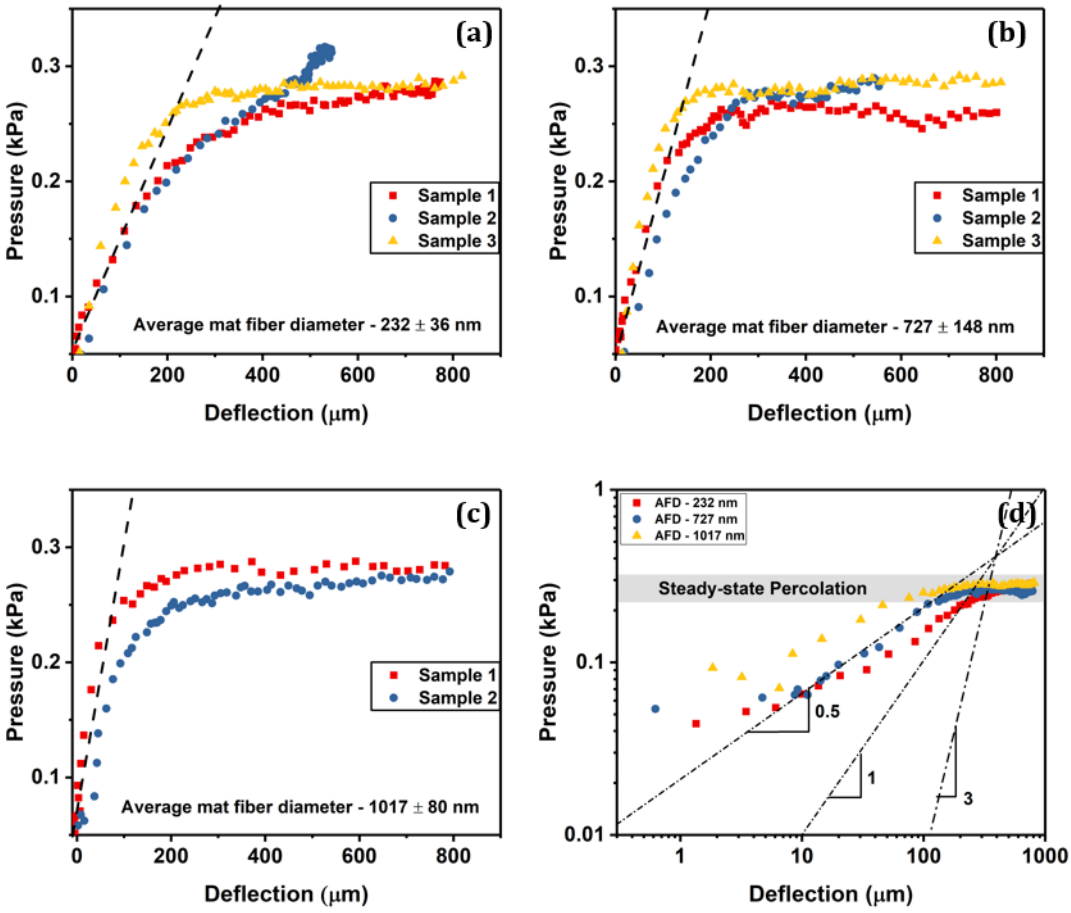

Figure 3: Representative pressure-deflection plots for the electrospun fiber mats. (a) Plot for mats with average fiber size of 232 nm and thickness of 29 μm (b) Plot for mats with average fiber size of 727 nm and thickness of 29.4 μm (c) Plot for mats with average fiber size of 1017 nm and thickness of 31μm (d) Plot showing the sub-linear relationship between the applied pressure and deflection for representative

Author accepted copy: Polymer, vol. 235, paper 124274 (8 pages) (2021) DOI: 10.1016/j.polymer.2021.124274

fiber mats. The dashed lines in (a), (b) and (c) are guides to show the average pressure - deflection response of the mat samples prior to percolation.

Due to uncertainties at the initial stages of the testing protocol (e.g. from sample clamping, pressure zeroing process, variations in mat wicking etc.) slight unsystematic variations were encountered at the beginning of each experiment. As a result, the pressure axes were offset by a small, finite value for consistency. In a broad sense, the bulge testing protocol is based on the application of uniform lateral pressure loading to edge–clamped planar geometries e.g. circular, rectangular and square plates. For the specific case of a circular geometry that's an elastic continuum, and under the assumptions of a linear elastic deformation and isotropic material properties, the classical constitutive model for the resultant pressure-deflection relationships is expressed as [38, 39]:

$$p = \frac{4\sigma_o t}{a^2} h + \frac{8Bt}{3a^4} h^3 \quad (1)$$

Where p, a, σ_o are the applied pressure, membrane half-length of the side, and residual stress, t is the thickness of the membrane, h is the out-of-plane deflection and B is the biaxial modulus which can be determined knowing the Young's modulus and Poisson's ratio, $E/(1-v)$. The pressure-deflection data is fitted to the model to extract a modulus and/or residual stress. The first term of eq.1 is related to the residual stress in the membrane. Neglecting effects of residual stresses reduces this to

$$p = \frac{8Bt}{3a^4} h^3 \quad (2)$$

and the cubic dependence between deflection and pressure ($p \sim h^3$) typifies membrane behavior dominated by mid-plane stretching in the membrane [40]. The validity of this model is contingent on the following conditions: the deflection is large compared to film thickness i.e. $h \gg t$; and the characteristic membrane dimension is much larger than the deflection i.e. $h \ll a$ [30, 38]. Implicit in the large deflection criterion is the presence of in-plane shear stresses which dominate the membrane response to the applied pressure, and consequently the contribution from the bending resistance, in effect, is negligible [41]. While the effective deflection of the electrospun fiber mats well exceeds their thickness as can be seen in figure 3a, b and c, their unique fiber assemblies exhibit a distinctive response to hydraulic flow-induced deformation

Author accepted copy: Polymer, vol. 235, paper 124274 (8 pages) (2021) DOI: 10.1016/j.polymer.2021.124274

wherein, system-scale shear stresses, and attendant stiffening effects [42], is expected to be minimal. This behavior is reflected in figure 3d where the data does not converge along the slope of 3 at large deflections. This is primarily due to a combination of factors based on: (1) the peculiar mat architecture, where membrane stresses may be relaxed through possible uncurling and translational motion of individual fibers and, (2) the orthogonal direction of fluid flow with respect to the plane of the freestanding mat may constrain the fibers to an initial out-of-plane bending deformation. Consequently, the pressure-induced transverse forces in the fiber mats may principally give rise to a bending-dominated response with possible attendant fiber sliding effects. It is well documented that small deformation of random cross-linked fibrous structures with relatively low densities (that are approximate to those in this study), wherein dramatic fiber reorientation and spatial reconfiguration is precluded, typically predict a non-affine network deformation with an attendant strain energy that is majorly accommodated by bending of the individual fibers [43]. In addition, the considerably high aspect ratio of the fibers minimizes the evolution of shear stresses during deformation as compared to bending stresses [43].

Alternatively, the elementary plate theory is based on the assumptions of pure bending and negligible membrane stresses, typically for small deflections $h \ll t$ [42]. The constitutive model for a circular plate deflection under an applied lateral pressure is then given as:

$$p = \frac{64D}{a^4} h \tag{3}$$

where, D is the plate bending rigidity. Here, a direct dependence exists between the applied pressure and deflection ($p \sim h$). From figure 3d, the data does not converge on the slope of 1 at small deflections. This does not disprove that the constitutive fibers undergo a bending response, but suggests that the deformation mechanics of the electrospun fiber mat is complex, and is different from what would be found with a monolithic membrane or plate.

The pressure-deflection relationships for the PAN fiber mats exhibited a non-linear relationship for the three distinct mat fiber diameters, exhibiting a sub-linear dependence with good agreement between the data points and the slope of 0.5, i.e. ($p \sim h^{\frac{1}{2}}$), figure 3d. A similar nonlinear response has been observed in the planar biaxial testing of nonwoven spunbonded fiber mats [44, 45]. This deformation response indicates that, while the applied pressure causes an out-of-plane deflection, it is being simultaneously dissipated as a consequence of the open cell architecture of the fiber mats. By way of contrast, the conventional deformation profile of

Author accepted copy: Polymer, vol. 235, paper 124274 (8 pages) (2021) DOI: 10.1016/j.polymer.2021.124274

monolithic thin films may take the form of a cubic parabola, indicative of progressive stiffening [28, 38, 46], or a straight line segment with a linear relationship, for plate-like behaviors [47].

Importantly, it is observed that for equivalent applied pressure, effective mat deflection increased with decreasing fiber size i.e. h (232 nm) > h (727 nm) > h (1017 nm), figure 3a, b, and c. This provides insights into the bending rigidity of the fiber mats to hydraulic flow. Furthermore, the transition to the plateau response is generally less abrupt or smoother in fiber mats with the smallest fiber size, that is, 232 nm, as compared to the other mats, underlining possible inertial effects during "yield". Given that the fiber mat thicknesses are relatively uniform across the fiber mats, and the areal densities are similar (and statistically equal), these mat attributes are assumed to be effectively equivalent across the mats, and the observed distinctions in deformation response prior to percolation may be ascribed to fiber dimension effects. As the mechanics of macroscopic mat deflection is, to a first approximation, an aggregation of single fiber mechanics, fiber bending provides insights that explain the disparities in the observed pressure-deflection response: if the fibers are considered as linear elastic rods with circular cross-sections that are consistent with the formulations of the classical Euler-Bernoulli beam theory [48], then beam flexural or bending rigidity is given as:

$$D = EI \tag{4}$$

Where E is the elastic modulus and I is the moment of inertia. For a circular cross-section, the moment of inertia is expressed as $\pi d^4/64$. Consequently a scaling relationship $D \sim d^4$ is established, showing a strong contribution of beam diameter on its rigidity. Therefore, beams with larger diameters possess a greater resistance to bending than beams with smaller diameters, taking into account that this dependence is modulated, on a system scale, by mat topology and porosity. In the same vein, for similar applied pressure, and neglecting differences in the moduli of the fibers, deflection reduces with increasing fiber size; from figure 3, it is evident that this manifests macroscopically in the deflection profiles of the fiber mats prior to steady-state percolation.

The nonlinear response of the fiber mats converge to a plateau region, but we must note that this is not necessarily a consequence of the material deformation, but results from a complete percolation of the hydraulic fluid, and the establishment of steady-state leakage or flow through the fiber mats. It has been shown that sudden bursts of discontinuous fiber motion dissipate imposed system or network–scale stresses [49], and this presumably might be an element of the mats' structural response that influences the transition to the plateau region or an effective

"yield"; and in conjunction with fiber bending, these effects enlarge the mat pores for steady-state leakage. The convergence of the plateau regions of the fiber mats may be explained by taking into consideration the mechanics of hydraulic flow through the fibrous networks: while the constitutive fibers are randomly oriented, it can be assumed that fluid flow is effectively transverse to the fibers' axes given the pseudo-two dimensional nature of the mats; and in idealized models of flow in fibrous media with uniform cross-sections, the drag force exerted by the fluid is given by [50]:

$$\frac{F}{\mu U} = \frac{\pi}{\phi}\left(\frac{r^2}{k}\right) \tag{5}$$

where F is the force per unit length exerted by an hydraulic fluid on fibers with radius r, μ is fluid viscosity, U is the mean fluid velocity, and ϕ and k are the solidity and permeability respectively. Furthermore, the permeability of a porous fibrous medium has been derived analytically as [14]:

$$k = \frac{r^2}{8\phi}\left(-\ln\phi + \frac{\phi^2 - 1}{\phi^2 + 1}\right) \tag{6}$$

Combining (5) and (6) yields

$$F \propto \frac{\pi\mu U}{f(\phi)} \tag{7}$$

where $f(\phi) = -\ln\phi + \frac{\phi^2-1}{\phi^2+1}$

The viscosity and flow velocity are constant in the testing protocol, so the drag force will be governed by the mat solidities. If the differences in the mat solidities are assumed negligible (given that the areal densities are also nominally similar), the drag forces developed on the fibrous architectures will be equivalent, and this presumably is the reason the applied pressure asymptotes at about the same values (plateau region) as steady state percolation is established. Coupling this to fiber deformation mechanics, the aforementioned processes of bending and fiber slippage occur in response to these drag effects, since the fibers are largely compliant and unrestricted, except at the mat edges where clamping was done.

Author accepted copy: Polymer, vol. 235, paper 124274 (8 pages) (2021) DOI: 10.1016/j.polymer.2021.124274

3.2. Effect of Mat thickness

In principle, varying the transverse thickness of a continuum material system may alter resultant pressure-deflection relationships; in particular, the influence stems from geometric ratios h/t and a/t that are strong determinants of whether membrane-like or plate-like deformation behaviors are obtained during uniform lateral pressure loading [47, 51]. For mats with average fiber diameters of 232 nm, figure 4 shows the deflection plot for a thickness of 52 μm superimposed on the 29 μm thick mat. We must note that testing a broader range of thicknesses within and across fiber diameters in a consistent and comparable manner proved challenging due to the stochastic nature of fiber deposition during electrospinning underpinned by natural jetting instabilities, and the intrinsic charge retention of PAN that undermines mat densification. Nevertheless, it can be seen that the deformation response prior to plateau is equivalent for both mat thicknesses. However, for the thicker mat, the transition to plateau is even much smoother, and a higher plateau pressure is observed in contrast to the mat with 29 μm thickness. As discussed previously, the commencement of translational motion of fibers as the applied pressure is increased is a necessary prelude to the plateau phenomenon; but, the convoluted structure of the fiber assembly translates to a considerable number of structural impediments generated by self-locking. Therefore, thicker mats should possess more "self-locks" or constraints to motion in the bulk, and this is probably responsible for the slightly greater pressure asymptote observed in figure 5. In addition, the higher areal density (~50% increase) may also translate to an increase in the exerted drag forces as discussed previously.

Author accepted copy: Polymer, vol. 235, paper 124274 (8 pages) (2021) DOI: 10.1016/j.polymer.2021.124274

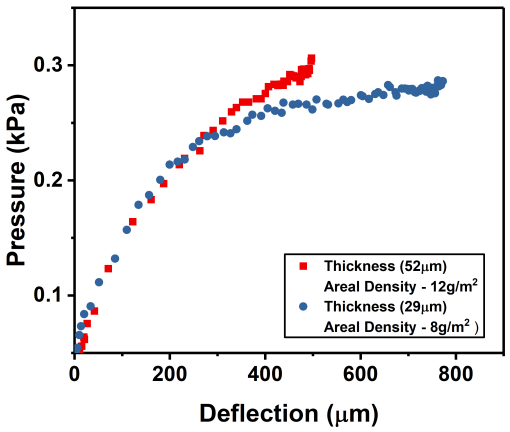

Figure 4: Pressure-deflection plot for fiber mats with the same average fiber size of 232 nm, but with distinct thicknesses of 52 μm and 29 μm

3.3. Effect of Flow rate

For elastic continua, deformation or strain rate effects may be introduced during testing by modulating the volumetric flow rate of the hydraulic fluid during quasi-static bulge testing [52]. The testing flow rate was systematically varied to evaluate effects on deflection profile of the fiber mats. These tests were carried out using a cyclic methodology: after characterization of each mat at a single flow rate, culminating in complete fluid percolation, a purge valve is opened to depressurize the system before successively testing at a higher flow rate, and the excess fluid on the mats is removed via capillary effects by delicately contacting the surface with laboratory tissue. Figure 5a and b show the deflection profiles under different flow rate regimes for the mats with fiber diameters of 232 nm and 1017 nm. The areal densities for both mats were on the same order, and average thicknesses were in the range of 29-31 μm. The consistent correspondence of the curves at all applied flow rates for both fiber mats shows that their deformation behavior is largely independent of the flow rate.

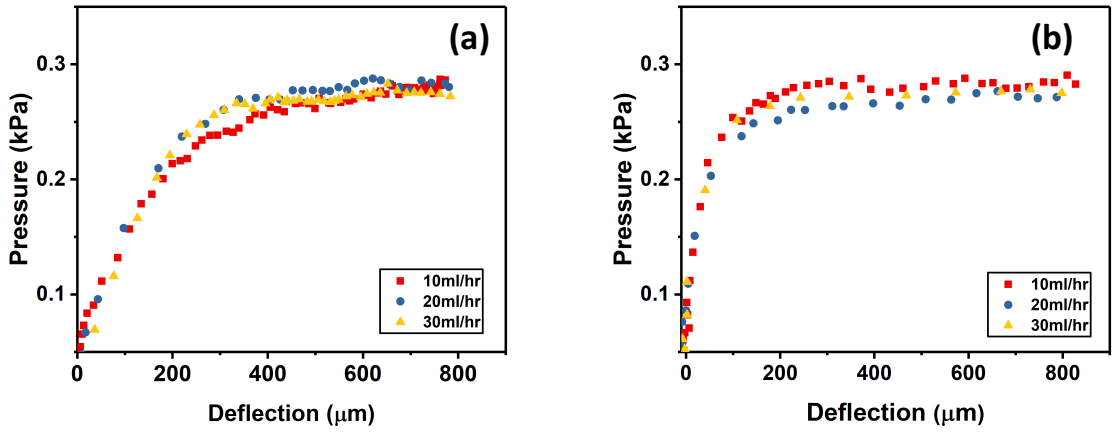

Figure 5: Effects of flow rates of 10 ml/hr, 20 ml/hr and 30 ml/hr on fiber mats of nominal thicknesses between 29-31μm (a) Average fiber diameters of 232 nm, and areal density of 8.1 g/m^2 (b) Average fiber diameters of 1017 nm, and areal density of 9.3 g/m^2

This may be interpreted in terms of the classical mechanics of fluid flow through a porous structure in relation to mat deformation. By definition, the hydraulic fluid, deionized water, possesses a viscous quality; as a result, work is done in pushing it through the "resistance" field of the porous fibrous network presented by the mats [53]. Since, water is a Newtonian fluid whose viscosity is constant with respect to variations in flow or shear rate, it is probable that the critical work being done at the distinct flow regimes are equivalent, with no noticeable effects on the mat deformation profile or response, but is strongly contingent on the geometry of the network as well as configuration. The lack of distinctive asymptote pressures or plateau regions with increasing flow rate (or fluid velocity) as predicted by equation 7 may be due to the infinitesimal differences between these flow conditions (on the order of ~10^{-6} m/s, using the chamber through – hole dimension of 0.0125 m as an effective flow cross – section). In addition, it can be deduced from these tests that the mats undergo minimal system-scale topological modifications after "yielding", and these are nominally reversible. Lastly, the deflection plots provide evidence that the induced bending strains in the constituent fibers are elastic or recoverable, with presumably minimal events of fiber buckling.

3.4. Comments

A caveat in the interpretation of our result is a consideration of the environment in which deflection takes place. Although the hydraulic liquid build-up provokes an out-of-plane mat deflection, it also provides a viscous medium that effectively encapsulates the deformation environment. As has been established, deformation can be considered as hierarchical: single fiber deflections facilitate macroscopic deformation of the mats. However, on a more fundamental level, the fluid viscosity will, in effect, impose some measure of retardation to these single fiber deflections at a given system pressure, and these mats may be more compliant in bending than suggested in these wet tests. Furthermore, in uniaxial tensile testing of electrospun fiber mats, a common observation is that hydration causes significant degradation in tensile strength and elastic rigidity due to moisture entrapment in between network pores as a result of lubricated fiber segments, enhancing sliding and slippage [54]. In contrast, the impact of the loading procedure in the leaky bulge test minimizes reorientation and fiber sliding-

Author accepted copy: Polymer, vol. 235, paper 124274 (8 pages) (2021) DOI: 10.1016/j.polymer.2021.124274

mediated deformation. Also, the plasticization of PAN by water molecules occurs only at moderately high temperatures [55], indicating that the fibers maintain an unadulterated chemical composition when wetted at room conditions. Hence, the structural and material integrity of PAN (or generally, polymer chemistries that are inert to water or hydration) are preserved during the leaky bulge test.

With the uniform application of lateral load, our interpretation has implied that the out-of-plane mat deformation geometry is convex, and the advancing water front during hydraulic pressurization (prior to steady-state percolation) is regular and conformal with this shape. Indeed, the inherent structural heterogeneity of the mats induces an irregular front [56] that could introduce geometric deviations in the bulged profiles of the mat that may be slightly different from that of a continuum plate or membrane, at least in prior to the plateau region, . Notwithstanding, the bending rigidities of the wet fiber mats provide added design factors for electrospun water filters and functional filters

4.0. CONCLUSION

In addition to good filtration efficiency, the maintenance of structural integrity of electrospun fiber mats is an important determinant of satisfactory application performance in terms of water filtration and sensing application. The compliant nature of the individual fibers as well as collective fiber assembly means electrospun water filters are susceptible to flow-induced bending deformation. We have adapted the hydraulic bulge testing procedure to quantify the resistance to flow-induced bending of wet electrospun polyacrylonitrile fiber mats.

In general, the pressure-deflection curves of the mats reveal a nonlinear response that is followed by a plateau region, corresponding to dissipation of imposed stresses and ultimate steady state leakage respectively. However, the pressure-deflection relationships of the mats, and by extension, bending resistance, are governed by the bending mechanics of constituent fibers. With increasing constituent fiber size, the rigidity of the mats of the mats increased. This observation highlights that the fibers approximate cylindrical beam wherein flexural rigidity increases with increasing beam/fiber cross-section as predicted by the Euler-Bernoulli beam theory, and this phenomenon manifests macroscopically in the random fiber assembly of the mats. Bending rigidity was largely unaffected by an increase in thickness, but a slightly higher pressure asymptote was observed. The cyclic flow rate test show that the bending rigidity is

Author accepted copy: Polymer, vol. 235, paper 124274 (8 pages) (2021) DOI: 10.1016/j.polymer.2021.124274

independent of flow rate and that bending strains and topological changes induced by hydraulic flow are reversible or recoverable.

Funding

This work was funded by the National Science Foundation under grant CMMI 1634772.

CRediT authorship contribution statement

Temitope Q. Aminu: Conceptualization, Data curation, Formal analysis, Investigation, Methodology, Software, Validation, Visualization, Writing – original draft, Writing – review & editing. David F.Bahr: Conceptualization, Formal analysis, Funding acquisition, Supervision.

Declaration of competing interest

The authors declare that they have no known competing financial interests or personal relationships that could have appeared to influence the work reported in this paper.

Author accepted copy: Polymer, vol. 235, paper 124274 (8 pages) (2021) DOI: 10.1016/j.polymer.2021.124274

References

[1] S. Ramakrishna, K. Fujihara, W.-E. Teo, T. Yong, Z. Ma, R. Ramaseshan, Electrospun nanofibers: solving global issues, Materials Today 9(3) (2006) 40-50.

[2] J. Xue, T. Wu, Y. Dai, Y. Xia, Electrospinning and Electrospun Nanofibers: Methods, Materials, and Applications, Chem. Rev. 119(8) (2019) 5298-5415.

[3] J. Xue, J.W. Xie, W. Liu, Y. Xia, Electrospun Nanofibers: New Concepts, Materials, and Applications, Accounts Chem. Res. 50(8) (2017) 1976-1987.

[4] T.H. Grafe, K.M. Graham, Nanofiber webs from electrospinning, pp. 1-5.

[5] A. Ridruejo, C. González, J. Llorca, Micromechanisms of deformation and fracture of polypropylene nonwoven fabrics, International Journal of Solids and Structures 48(1) (2011) 153-162.

[6] C. Poorya, R. Mir Jalil, Effect of the Interfiber Bonding on the Mechanical Behavior of Electrospun Fibrous Mats, Scientific reports 10(1) (2020) 1-10.

[7] F. Martínez-Hergueta, A. Ridruejo, C. González, J. Llorca, Deformation and energy dissipation mechanisms of needle-punched nonwoven fabrics: A multiscale experimental analysis, International Journal of Solids and Structures 64-65 (2015) 120-131.

[8] P. Jearanaisilawong, A continuum model for needlepunched nonwoven fabrics, (2008).

[9] E. Vatankhah, D. Semnani, M.P. Prabhakaran, M. Tadayon, S. Razavi, S. Ramakrishna, Artificial neural network for modeling the elastic modulus of electrospun polycaprolactone/gelatin scaffolds, Acta Biomaterialia 10(2) (2014) 709-721.

[10] C.T. Koh, C.Y. Low, Y.B. Yusof, Structure-property Relationship of Bio-Inspired Fibrous Materials, Procedia Computer Science 76(C) (2015) 411-416.

[11] S. Kaur, R. Barhate, S. Sundarrajan, T. Matsuura, S. Ramakrishna, Hot pressing of electrospun membrane composite and its influence on separation performance on thin film composite nanofiltration membrane, Desalination 279(1-3) (2011) 201-209.

[12] L. Huang, S.S. Manickam, J.R. McCutcheon, Increasing strength of electrospun nanofiber membranes for water filtration using solvent vapor, Journal of membrane science 436 (2013) 213-220.

[13] N.E. Zander, M. Gillan, D. Sweetser, Recycled PET Nanofibers for Water Filtration Applications, Materials (Basel) 9(4) (2016) 247.

[14] L.T. Choong, Z. Khan, G.C. Rutledge, Permeability of electrospun fiber mats under hydraulic flow, Journal of Membrane Science 451(C) (2014) 111-116.

[15] D. Bjorge, N. Daels, S. De Vrieze, P. Dejans, T. Van Camp, W. Audenaert, J. Hogie, P. Westbroek, K. De Clerck, S.W.H. Van Hulle, Performance assessment of electrospun nanofibers for filter applications, Desalination 249(3) (2009) 942-948.

Author accepted copy: Polymer, vol. 235, paper 124274 (8 pages) (2021) DOI: 10.1016/j.polymer.2021.124274

[16] B.-Y. Chen, C.-C. Kuo, C.-J. Cho, F.-C. Liang, R.-J. Jeng, Novel fluorescent chemosensory filter membranes composed of electrospun nanofibers with ultra-selective and reversible pH and Hg2+ sensing characteristics, Dyes and Pigments 143 (2017) 129-142.
[17] L.Y. Wan, H. Wang, W. Gao, F. Ko, An analysis of the tensile properties of nanofiber mats, Polymer 73 (2015) 62-67.
[18] E.P.S. Tan, C.T. Lim, Mechanical characterization of nanofibers – A review, Composites Science and Technology 66(9) (2006) 1102-1111.
[19] S. Chew, T.C. Hufnagel, C.T. Lim, K. Leong, Mechanical properties of single electrospun drug-encapsulated nanofibres, Nanotechnology 17(15) (2006) 3880-3891.
[20] E.P.S. Tan, C.N. Goh, C.H. Sow, C.T. Lim, Tensile test of a single nanofiber using an atomic force microscope tip, Applied Physics Letters 86(7) (2005).
[21] M.N. Silberstein, C.-L. Pai, G.C. Rutledge, M.C. Boyce, Elastic–plastic behavior of non-woven fibrous mats, Journal of the Mechanics and Physics of Solids 60(2) (2012) 295-318.
[22] W.-J. Li, J.A. Cooper, R.L. Mauck, R.S. Tuan, Fabrication and characterization of six electrospun poly(α-hydroxy ester)-based fibrous scaffolds for tissue engineering applications, Acta Biomaterialia 2(4) (2006) 377-385.
[23] J. Maksimcuka, A. Obata, W.W. Sampson, R. Blanc, C. Gao, P.J. Withers, O. Tsigkou, T. Kasuga, P.D. Lee, G. Poologasundarampillai, X-ray Tomographic Imaging of Tensile Deformation Modes of Electrospun Biodegradable Polyester Fibers, Frontiers in Materials 4 (2017).
[24] N.J. Amoroso, A. D'Amore, Y. Hong, W.R. Wagner, M.S. Sacks, Elastomeric electrospun polyurethane scaffolds: the interrelationship between fabrication conditions, fiber topology, and mechanical properties, Advanced materials (Deerfield Beach, Fla.) 23(1) (2011) 106.
[25] Y. Yin, J. Xiong, Finite Element Analysis of Electrospun Nanofibrous Mats under Biaxial Tension, Nanomaterials 8(5) (2018) 348.
[26] Z. Hua, W. Hongxia, N. Haitao, L. Tong, Electrospun Fibrous Membranes with Super-large-strain Electric Superhydrophobicity, Scientific Reports 5(1) (2015).
[27] T.P. Driscoll, R.H. Nakasone, S.E. Szczesny, D.M. Elliott, R.L. Mauck, Biaxial mechanics and inter-lamellar shearing of stem-cell seeded electrospun angle-ply laminates for annulus fibrosus tissue engineering, Journal of Orthopaedic Research 31(6) (2013) 864-870.
[28] J. Vlassak, W. Nix, New Bulge Test Technique for the Determination of Young's Modulus and Poisson's Ratio of Thin Films, Journal of Materials Research 7(12) (1992) 3242-3249.
[29] D.W. Zheng, Y.H. Xu, Y.P. Tsai, K.N. Tu, P. Patterson, B. Zhao, Q.Z. Liu, M. Brongo, Mechanical property measurement of thin polymeric-low dielectric-constant films using bulge testing method, Applied Physics Letters 76(15) (2000) 2008-2010.

Author accepted copy: Polymer, vol. 235, paper 124274 (8 pages) (2021) DOI: 10.1016/j.polymer.2021.124274

[30] Y. Xiang, X. Chen, J. Vlassak, Plane-strain bulge test for thin films, Journal of Materials Research 20(9) (2005) 2360-2370.
[31] T.K. Tonge, L.S. Atlan, L.M. Voo, T.D. Nguyen, Full-field bulge test for planar anisotropic tissues: Part I – Experimental methods applied to human skin tissue, Acta Biomaterialia 9(4) (2013) 5913-5925.
[32] F. Rossi, F. Fumagalli, A. Ruiz-Moreno, P. Moilanen, P. Hähner, Membrane bulge test rig for irradiation-assisted stress-corrosion cracking, Nuclear instruments & methods in physics research. Section B, Beam interactions with materials and atoms 479 (2020) 80-92.
[33] R. Roche, F. Yalcinkaya, Electrospun Polyacrylonitrile Nanofibrous Membranes for Point-of-Use Water and Air Cleaning, ChemistryOpen 8(1) (2019) 97-103.
[34] S. Parekh, R. David, K. Bannuru, L. Krishnaswamy, A. Baji, Electrospun Silver Coated Polyacrylonitrile Membranes for Water Filtration Applications, Membranes (Basel) 8(3) (2018) 59.
[35] Z. Zhou, C. Lai, L. Zhang, Y. Qian, H. Hou, D.H. Reneker, H. Fong, Development of carbon nanofibers from aligned electrospun polyacrylonitrile nanofiber bundles and characterization of their microstructural, electrical, and mechanical properties, Polymer 50(13) (2009) 2999-3006.
[36] T. Wang, S. Kumar, Electrospinning of polyacrylonitrile nanofibers, Journal of applied polymer science 102(2) (2006) 1023-1029.
[37] J.-H. He, Y.-Q. Wan, J.-Y. Yu, Effect of concentration on electrospun polyacrylonitrile (PAN) nanofibers, Fibers and polymers 9(2) (2008) 140-142
[38] M. Small, W. Nix, Analysis of the Accuracy of the Bulge Test in Determining the Mechanical-Properties of Thin-Films, J. Mater. Res. 7(6) (1992) 1553-1563.
[39] K.S. Chen, K.S. Ou, MEMS Residual Stress Characterization: Methodology and Perspective, 2015.
[40] Z. Cao, A blister test for interfacial adhesion of large-scale transferred graphene, Carbon 69 (2014) 390-401.
[41] Film stress and substrate curvature, in: L.B. Freund, S. Suresh (Eds.), Thin Film Materials: Stress, Defect Formation and Surface Evolution, Cambridge University Press, Cambridge, 2004, pp. 86-153.
[42] S. Timoshenko, Theory of plates and shells, 2d ed. ed., McGraw-Hill, New York, 1959.
[43] R.C. Picu, Mechanics of random fiber networks—a review, Soft matter 7(15) (2011) 6768.
[44] A. Rawal, A. Kochhar, A. Gupta, Biaxial tensile behavior of spunbonded nonwoven geotextiles, Geotextiles and Geomembranes 29(6) (2011) 596-599.
[45] S. Bais-Singh, B.C. Goswami, Predicting the Biaxial Tensile Deformation Behavior of Spunbonded Nonwovens, Textile Research Journal 68(3) (1998) 219-227.

Author accepted copy: Polymer, vol. 235, paper 124274 (8 pages) (2021) DOI: 10.1016/j.polymer.2021.124274

[46] M.S. Kennedy, A.L. Olson, J.C. Raupp, N.R. Moody, D.F. Bahr, Coupling bulge testing and nanoindention to characterize materials properties of bulk micromachined structures, Microsystem technologies : sensors, actuators, systems integration 11(4) (2005) 298-302.
[47] Z. Cao, L. Tao, D. Akinwande, R. Huang, K.M. Liechti, Mixed-mode traction-separation relations between graphene and copper by blister tests, International journal of solids and structures 84 (2016) 147-159.
[48] C.M. Wang, J.N. Reddy, K.H. Lee, Shear Deformable Beams and Plates, Elsevier Science & Technology, Elsevier Science, Oxford, 2000.
[49] J.A. Ketoja, S. Paunonen, P. Jetsu, E. Pääkkönen, Compression Strength Mechanisms of Low-Density Fibrous Materials, Materials (Basel) 12(3) (2019) 384.
[50] T. Stylianopoulos, A. Yeckel, J.J. Derby, X.-J. Luo, M.S. Shephard, E.A. Sander, V.H. Barocas, Permeability calculations in three-dimensional isotropic and oriented fiber networks, Phys Fluids (1994) 20(12) (2008) 123601-123601.
[51] E.A. Ventsel, T.A. Krauthammer, E.R. Carrera, Thin Plates and Shells: Theory, Analysis, and Applications, Applied Mechanics Reviews 55(4) (2002) B72-B73.
[52] S. Kaya, T. Altan, P. Groche, C. Klöpsch, Determination of the flow stress of magnesium AZ31-O sheet at elevated temperatures using the hydraulic bulge test, International journal of machine tools & manufacture 48(5) (2008) 550-557.
[53] L.J. Gibson, Cellular solids : structure and properties, 2nd ed., 1st pbk. ed. with corr. ed., Cambridge University Press, Cambridge ; New York, 1999.
[54] K.L. Goh, M. Makaremi, P. Pasbakhsh, R.T. De Silva, V. Zivkovic, Direct measurement of the elasticity and fracture properties of electrospun polyacrylonitrile/halloysite fibrous mesh in water, Polymer Testing 72 (2018) 11-23.
[55] Z. Bashir, S.P. Church, D. Waldron, Interaction of water and hydrated crystallization in water-plasticized polyacrylonitrile films, Polymer (Guilford) 35(5) (1994) 967-976.
[56] M. Alava, K. Niskanen, The physics of paper, Reports on progress in physics 69(3) (2006) 669-723.

Author accepted copy: Polymer, vol. 235, paper 124274 (8 pages) (2021) DOI: 10.1016/j.polymer.2021.124274